ISSN 1070-3284, Russian Journal of Coordination Chemistry, 2015, Vol. 41, No. 7, pp. 469–480. © Pleiades Publishing, Ltd., 2015.

Synthesis, Crystal Structure, and Porosity of 1D Coordination Polymer of Neodymium(III) with Isonicotinic Acid and Dimeric Complex of Neodymium(III) with Nicotinic Acid[1]

S. Sharma, M. Yawer, M. Kariem, R. Singh, and H. N. Sheikh*

Post-Graduate Department of Chemistry, University of Jammu, Baba Sahib Ambedkar Road, Jammu Taw, 180006 India

**e-mail: hnsheikh@rediffmail.com*

Received November 1, 2014

Abstract—A 1D coordination polymer $[Nd_3(INA)_9(H_2O)_6]_n$ (**I**) and a dimeric complex with mononuclear asymmetric unit $[Nd(NA)_3(H_2O)_2]$ (**II**) (HINA = isonicotinic acid and HNA = nicotinic acid) were synthesized. The compounds were characterized by elemental analyses, infrared spectroscopy and single crystal X-ray diffraction studies (CIF file CCDC nos. 938976 (**I**) and 939061 (**II**). X-ray crystal structure analysis reveals that both compounds exhibit rich structural chemistry. Compounds **I** and **II** belong to the monoclinic system with space group $P2_1/c$. Thermogravimetric analysis has been performed to investigate their thermal stability. The coordination polymer **I** has meso-porous structure with average diameter of pores (~4 nm) and BET surface area 13.62 m^2/g.

DOI: 10.1134/S1070328415060068

INTRODUCTION

Lanthanide coordination polymers have currently provoked considerable interest owing to their enormous variety of intriguing structural topologies as well as great potential applications in the areas of catalysis [1–3], gas storage [4], separation [5], magnetism [6, 7], and luminescence [8, 9]. Large number of lanthanide metal organic frameworks (MOFs) with various structures and interesting properties have been obtained by the self-assembly of metal ions and organic ligands [10–13]. The design and control over lanthanides based frameworks are strongly influenced by various factors such as organic ligands [14], systematic pH value [15, 16], template effect [17], and reaction temperature [18]. The synthesis and functionality of MOFs and self-assembled supramolecular coordination complexes have been recently reviewed [19, 20]. Lanthanide ions have high affinity for ligands containing oxygen or hybrid oxygen–nitrogen atoms. Lanthanide ions are known to form condensed structures due to their high coordination numbers and flexible coordination environments [21–23]. Because of these characteristics, lanthanides ions are best choices to develop high-dimensional MOFs through self-assembly processes. However, design and control of lanthanide based high-dimensional frameworks are more difficult in contrast to transition metal polymers [24].

Multicarboxylate ligands are usually employed in the architectures of lanthanide coordination polymers with unique structure and useful properties. The heterocyclic aromatic carboxylic acid, such as isonicotinic acid and nicotinic acid can bridge metal ions together using both N-donors from pyridine ring and O-donors from the carboxyl group [25]. On the basis of above mentioned considerations, we selected isonicotinic acid and nicotinic acid as potential linker between lanthanides metal ions. A variety of metal organic frameworks of transition metal with isonicotinic acid and nicotinic acid have been reported [26–28], but the reports on the lanthanides MOF with such heterocyclic ligands are rare. In continuation of our work on coordination polymers with multifunctional ligands [29, 30], we report here the systematic synthesis and structures of two Nd(III) coordination frameworks by using isonicotinic acid (HINA) and nicotinic acid (HNA) as ligands under hydrothermal conditions.

EXPERIMENTAL

Materials and methods. All materials used for synthesis were of reagent grade and used without further purification. Neodymium nitrate hexahydrate was purchased from Alfa Aesar. Nicotinic acid and isonicotinic acid were purchased from Sigma Aldrich. The Fourier Transform Infrared spectra were recorded in the range 4000–400 cm^{-1} on PerkinElmer-Spectrum RX-IFTIR spectrophotometer with solid KBr pellets. C, H, and N microanalyses were carried out on CHNS-932 Leco elemental analyzer. Thermogravimetric analysis (TGA-DTA) was carried out on Met-

[1] The article is published in the original.

Table 1. Crystallographic data and structure refinement for complexes **I** and **II**

Parameter	Value	
	I	**II**
Formula weight	1637.72	546.58
Crystal system	Monoclinic	Monoclinic
Space group	$P2_1/c$	$P2_1/c$
a, Å	11.9973(2)	9.65980(10)
b, Å	19.7599(3)	12.00480(10)
c, Å	26.0246(5)	17.1045(2)
β, deg	91.683(2)	93.2370(10)
V, Å	6166.87(18)	1980.34(4)
Z	4	4
μ, mm^{-1}	2.575	2.673
Limiting indices hkl	$-14 \le h \le 14$, $-23 \le k \le 23$, $-29 \le l \le 30$	$-11 \le h \le 11$, $-14 \le k \le 13$, $-20 \le l \le 20$
Total reflection	52296	16321
Unique reflection	10845	3486
R_{int}	0.0184	0.0181
Parameters/restraints	927/9	287/4
$R(F_o)$ for $F_o^2 > 2\sigma(F_o^2)$*	0.0480	0.0135
$Rw(F_o^2)$*	0.1105	0.03200
$\Delta\rho_{max}/\Delta\rho_{min}$, e Å^3	1.621/−3.751	0.380/−0.304
Goodness-of-fit	1.063	1.038

* $R(F_o) = \Sigma\|F_o| - |F_c\|/\Sigma|F_o|$; $Rw(F_o^2) = [\Sigma[w(F_o^2 - F_c^2)^2]/\Sigma F_o 4]^{1/2}$.

tler Toledo TGA/SDTA 851e in nitrogen atmosphere with a heating rate of 10°C min^{-1}.

Synthesis of $[Nd_3(INA)_9(H_2O)_6]_n$ (I). The 5 mL aqueous solution of $Nd(NO_3)_3 \cdot 6H_2O$ (0.2199 g, 0.5 mmol) was added drop wise to 10 mL aqueous solution of isonicotinic acid (HINA) (0.184 g, 1.5 mmol), and the pH value was adjusted to about 6.5 with NaOH. The mixture was stirred for 2 h. The resulting solution was filtered and the filtrate was allowed to stand at room temperature. After one week, purple crystals of I suitable for X-ray single crystal diffraction analysis were obtained. The yield was ~0.160 g (59%) based on Nd.

For $C_{54}H_{46}N_9O_{24}Nd_3$

anal. calcd., %:	C, 39.60;	H, 2.83;	N, 7.70.
Found, %:	C, 39.67;	H, 2.70;	N, 7.58.

IR (ν, cm^{-1}): 3300 m, br, 3087 w, 2430 m, 1956 w, br, 1628 m, 1586 s, 1539 s, 1496 w, 1405 s, 1224 s, 1060 s, 1006 s, 862 s, 769 s, 686 s, 534 m.

Synthesis of $[Nd(NA)_3(H_2O)_2]$ (II). The synthetic procedure used to synthesize **II** was same as that for **I** except that ligand HNA (0.184 g, 1.5 mmol) was used instead of HINA to obtain purple crystals of **II**. The yield was ~0.166 g (61%) based on Nd.

For $C_{18}H_{16}N_3O_8Nd$

anal. calcd., %:	C, 39.55;	H, 2.95;	N, 7.69.
Found, %:	C, 39.59;	H, 2.80;	N, 7.55.

IR (ν, cm^{-1}): 3363 w, br, 3095 w, 2427 w, 1628 s, 1598 s, 1541 s, 1477 w, 1432 w, 1402 w, 1246 w, 1196 s, 1159 s, 1093 s, 1027 s, 858 s, 769 s, 703 s, 634 s, 557 m.

X-ray structures determination. Single crystal X-ray diffraction measurements were performed on a CCD Agilent Technologies (Oxford Diffraction) SUPER NOVA diffractometer. Data were collected at 150(2) K using graphite-monochromated MoK_α radiation (λ = 0.71073 Å). The strategy for data collection was evaluated by using the CrysAlisPro CCD software. The data were collected by standard θ–ω scan techniques, and were scaled and reduced using CrysAlisPro RED software. Data was corrected for Lorentz, polarisation and absorption factors. The structures were solved by direct methods using SHELXS-97 [31] and refined by full matrix least-squares with SHELXL-97, refining on F^2 [32]. The positions of all the atoms were obtained by direct methods. All non-H-atoms were refined anisotropically. The remaining H atoms were placed in geometrically constrained positions and refined with isotropic temperature factors, generally 1.2U_{eq} of their parent atoms. The crystal and refinement data are summarized in Table 1. Selected bond distances and bond angles are shown in Tables 2 and 3.

Supplementary material has been deposited with the Cambridge Crystallographic Data Centre (nos. 938976 (**I**) and 939061 (**II**); deposit@ccdc.cam.ac.uk or http://www.ccdc.cam.ac.uk).

Table 2. Selected bond distances (Å) and angles (deg) for **I**

Bond	*d*, Å	Bond	*d*, Å
Nd(1)–O(8)	2.400(4)	Nd(2)–O(9)	2.467(3)
Nd(1)–O(7)	2.412(4)	Nd(2)–O(12)	2.472(4)
Nd(1)–O(3)	2.412(4)	Nd(2)–O(16)	2.509(3)
Nd(1)–O(2)	2.457(5)	Nd(2)–O(15)	2.517(4)
Nd(1)–O(6)	2.461(4)	Nd(3)–O(18)	2.396(4)
Nd(1)–O(5)	2.467(4)	Nd(3)–O(21)	2.420(4)
Nd(1)–O(1)	2.533(4)	Nd(3)–O(23)	2.437(4)
Nd(1)–O(4)	2.551(4)	Nd(3)–O(19)	2.460(4)
Nd(2)–O(10)	2.410(3)	Nd(3)–O(20)	2.463(4)
Nd(2)–O(14)	2.412(4)	Nd(3)–O(17)	2.465(4)
Nd(2)–O(11)	2.415(4)	Nd(3)–O(24)	2.522(4)
Nd(2)–O(13)	2.461(3)	Nd(3)–O(22)	2.540(4)
Angle	ω, deg	Angle	ω, deg
O(8)Nd(1)O(7)	93.66(14)	O(9)Nd(2)O(12)	142.21(13)
O(8)Nd(1)O(3)	83.66(14)	O(10)Nd(2)O(16)	139.79(14)
O(7) Nd(1)O(3)	145.02(15)	O(14) Nd(2)O(16)	72.42(14)
O(8)Nd(1)O(2)	83.44(15)	O(11)Nd(2)O(16)	77.75(14)
O(7)Nd(1)O(2)	143.08(14)	O(13)Nd(2)O(16)	71.14(13)
O(3)Nd(1)O(2)	71.46(15)	O(9)Nd(2)O(16)	69.65(13)
O(8)Nd(1)O(6)	139.95(14)	O(12)Nd(2)O(16)	140.53(14)
O(7)Nd(1)O(6)	78.49(13)	O(10)Nd(2)O(15)	70.69(13)
O(3)Nd(1)O(6)	81.41(14)	O(14)Nd(2)O(15)	73.33(14)
O(2)Nd(1)O(6)	125.52(14)	O(11)Nd(2)O(15)	136.72(13)
O(8)Nd(1)O(5)	140.41(15)	O(13)Nd(2)O(15)	141.74(14)
O(7)Nd(1)O(5)	82.17(15)	O(9)Nd(2)O(15)	71.60(13)
O(3)Nd(1)O(5)	121.08(15)	O(12)Nd(2)O(15)	71.59(14)
O(2)Nd(1)O(5)	77.30(16)	O(16)Nd(2)O(15)	122.27(14)
O(6)Nd(1)O(5)	77.98(15)	O(18)Nd(3)O(21)	147.42(14)
O(8)Nd(1)O(1)	71.12(14)	O(18)Nd(3)O(23)	84.58(13)
O(7)Nd(1)O(1)	72.86(15)	O(21)Nd(3)O(23)	94.80(14)
O(3)Nd(1)O(1)	136.90(16)	O(18)Nd(3)O(19)	80.60(14)
O(2)Nd(1)O(1)	71.40(14)	O(21)Nd(3)O(19)	79.06(14)
O(6)Nd(1)O(1)	139.28(14)	O(23)Nd(3)O(19)	139.70(14)
O(5)Nd(1)O(1)	70.05(15)	O(18)Nd(3)O(20)	120.82(14)
O(8)Nd(1)O(4)	69.79(15)	O(21)Nd(3)O(20)	79.53(15)
O(7)Nd(1)O(4)	71.17(15)	O(23)Nd(3)O(20)	139.83(14)
O(3)Nd(1)O(4)	75.25(16)	O(19)Nd(3)O(20)	78.72(15)
O(2)Nd(1)O(4)	139.11(15)	O(18)Nd(3)O(17)	70.34(13)
O(6)Nd(1)O(4)	70.53(14)	O(21)Nd(3)O(17)	141.96(14)
O(5)Nd(1)O(4)	141.90(15)	O(23)Nd(3)O(17)	81.93(13)
O(1)Nd(1)O(4)	123.86(14)	O(19)Nd(3)O(17)	126.41(13)
O(10)Nd(2)O(14)	141.76(13)	O(20)Nd(3)O(17)	79.14(15)
O(10)Nd(2)O(11)	71.24(13)	O(18)Nd(3)O(24)	78.10(14)
O(14)Nd(2)O(11)	147.00(13)	O(21)Nd(3)O(24)	71.39(14)
O(10)Nd(2)O(13)	124.74(13)	O(23)Nd(3)O(24)	69.08(13)
O(14)Nd(2)O(13)	78.70(13)	O(19)Nd(3)O(24)	71.26(13)
O(11)Nd(2)O(13)	78.58(13)	O(20)Nd(3)O(24)	141.30(15)
O(10)Nd(2)O(9)	81.69(13)	O(17)Nd(3)O(24)	138.78(13)
O(14)Nd(2)O(9)	98.99(13)	O(18)Nd(3)O(22)	136.48(14)
O(11)Nd(2)O(9)	83.28(13)	O(21)Nd(3)O(22)	71.84(15)
O(13)Nd(2)O(9)	139.40(12)	O(23)Nd(3)O(22)	70.10(15)
O(10)Nd(2)O(12)	78.45(13)	O(19)Nd(3)O(22)	140.55(15)
O(14)Nd(2)O(12)	78.35(14)	O(20)Nd(3)O(22)	70.38(16)
O(11)Nd(2)O(12)	119.29(14)	O(17)Nd(3)O(22)	71.46(14)
O(13)Nd(2)O(12)	77.66(13)	O(24)Nd(3)O(22)	121.18(16)

Table 3. Selected bond distances (Å) and angles (deg) for **II***

Bond	*d*, Å	Bond	*d*, Å
Nd(1)–O(6)	2.4092(13)	Nd(1)–O(3)	2.4781(14)
Nd(1)–O(4)	2.4379(12)	Nd(1)–O(2)	2.5127(13)
Nd(1)–O(5)	2.4483(13)	Nd(1)–O(1)	2.5982(13)
Nd(1)–O(8)	2.4530(13)	Nd(1)–O(5)^{i}	2.8935(14)
Nd(1)–O(7)	2.4553(15)		
Angle	ω, deg	Angle	ω, deg
O(6)Nd(1)O(4)	132.90(4)	O(8)Nd(1)O(2)	89.91(5)
O(6)Nd(1)O(5)	72.27(5)	O(7)Nd(1)O(2)	68.78(5)
O(4)Nd(1)O(5)	74.53(4)	O(3)Nd(1)O(2)	139.39(5)
O(6)Nd(1)O(8)	145.93(5)	O(6)Nd(1)O(1)	120.76(5)
O(4)Nd(1)O(8)	75.83(5)	O(4)Nd(1)O(1)	84.65(4)
O(5)Nd(1)O(8)	141.28(5)	O(5)Nd(1)O(1)	80.30(4)
O(6)Nd(1)O(7)	71.48(5)	O(8)Nd(1)O(1)	72.63(5)
O(4)Nd(1)O(7)	141.12(5)	O(7)Nd(1)O(1)	109.45(5)
O(5)Nd(1)O(7)	142.10(5)	O(3)Nd(1)O(1)	141.42(4)
O(8)Nd(1)O(7)	74.49(5)	O(2)Nd(1)O(1)	50.92(4)
O(6)Nd(1)O(3)	96.66(5)	O(6)Nd(1)O(5)^{i}	70.19(4)
O(4)Nd(1)O(3)	75.16(5)	O(4)Nd(1)O(5)^{i}	70.75(4)
O(5)Nd(1)O(3)	123.53(5)	O(5)Nd(1)O(5)^{i}	77.56(5)
O(8)Nd(1)O(3)	70.73(5)	O(8)Nd(1)O(5)^{i}	114.91(4)
O(7)Nd(1)O(3)	71.70(5)	O(7)Nd(1)O(5)^{i}	100.06(5)
O(6)Nd(1)O(2)	79.52(5)	O(3)Nd(1)O(5)^{i}	47.69(4)
O(4)Nd(1)O(2)	135.55(4)	O(2)Nd(1)O(5)^{i}	149.70(4)
O(5)Nd(1)O(2)	94.10(5)	O(1)Nd(1)O(5)^{i}	150.43(4)

* Symmetry code: ^{i} $-x + 2, -y, -z$.

N_2 TPD and BET surface area. The specific surface area, total pore volume and average pore diameter were measured by N_2 adsorption–desorption method using a NOVA 1200 (Quanta chrome) instrument. The bath temperature was maintained at 77 K. The sample was degassed at 423 K for 12 h before measurement. Pore size distribution and pore volume were obtained by applying the Barrett–Joyner–Halenda (BJH) analysis to the adsorption branch of the nitrogen adsorption–desorption isotherms. The specific surface area of the sample was calculated using the BET method. Micropore surface area and micropore volume were determined from t-plot analysis. All the flow rates were maintained at normal temperature and pressure.

RESULTS AND DISCUSSION

The reaction of $Nd(NO_3)_3 \cdot 6H_2O$ with the requisite heterocyclic aromatic carboxylic acid in water under controlled pH resulted in formation of purple colored crystals of coordination polymer **I** and dinuclear complex **II**. Both polymer **I** and complex **II** are stable in air and have been characterized by elemental analysis, FT–IR spectroscopy, single-crystal X-ray diffraction, N_2 TPD-BET surface area and TGA studies.

FT–IR spectra of **I** and **II** show indicative vibrational bands of carboxylate groups and water molecules Broad, weak spectral bands in the vicinity of 3050–3400 cm^{-1} and strong band at 1628 cm^{-1} are attributed to ν(O–H) and δ(H_2O) modes of coordinated water molecules, respectively. Sharp bands at 862 cm^{-1} for **I** and 858 cm^{-1} for **II** are assigned to $\rho_r(H_2O)$ rocking mode of coordinated water whereas weak bands at 534 cm^{-1} for **I** and 557 cm^{-1} for **II** are contributed by $\rho_w(H_2O)$ wagging modes of coordinated water molecule. Intense, slightly broadened bands due to ν_{as}(COO) and ν_s(COO) were observed at 1586 and 1405 cm^{-1} in **I** and 1598 and 1402 cm^{-1} in **II**. The $\nu_{as} - \nu_s$ is 181 and 196 cm^{-1} in **I** and **II**, respectively. Sharp and strong bands were observed at 1590 and 1432 cm^{-1} in **II** which also can be assigned to ν_{as}(COO) and ν_s(COO). The $\Delta\nu = \nu_{as} - \nu_s$ for this pair is 158 cm^{-1}. The value of $\Delta\nu = 181$ cm^{-1} in **I** indicates that carboxylato group of isonicotinate anion is bonded in bridging mode whereas values of $\Delta\nu = 196$ and 158 cm^{-1} in **II** suggest that carboxylate groups are bonded in bidentate bridging as well as bidentate chelating mode [33, 34]. The in-plane δ(OCO) vibration modes appear as sharp bands at 686 and 703 cm^{-1} for **I** and **II**, respectively. Absorption band at 1496 and 1477 cm^{-1} are assigned to ν(C=N) of pyridine ring of **I** and **II**, respectively.

The asymmetric unit of **I** consists of three crystallographically independent Nd^{3+} sites [Nd(1), Nd(2), Nd(3)], nine INA^- fragments and six coordinated

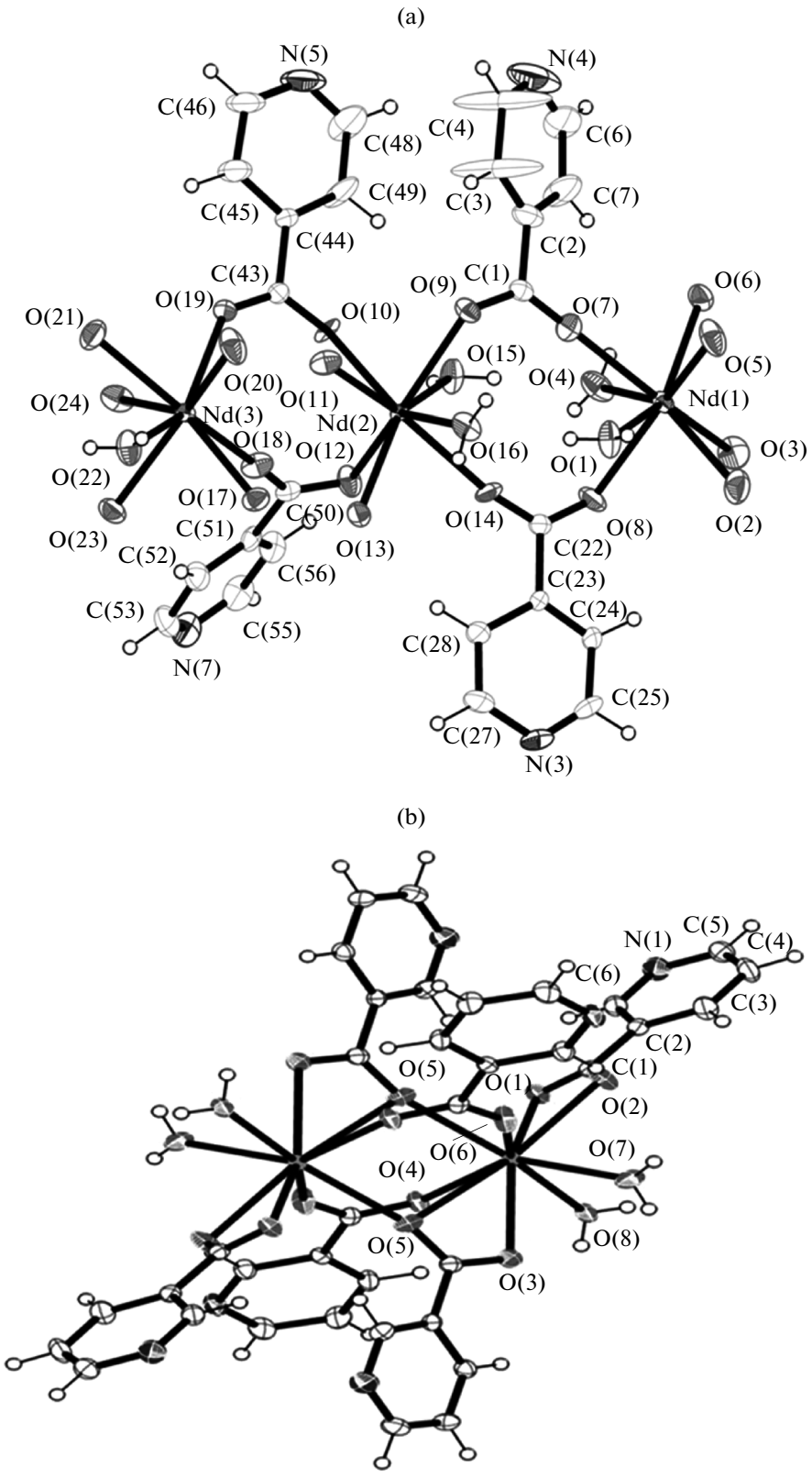

Fig. 1. ORTEP diagram of **I** (a) and **II** (b) with displacement ellipsoids drawn at 50% probability.

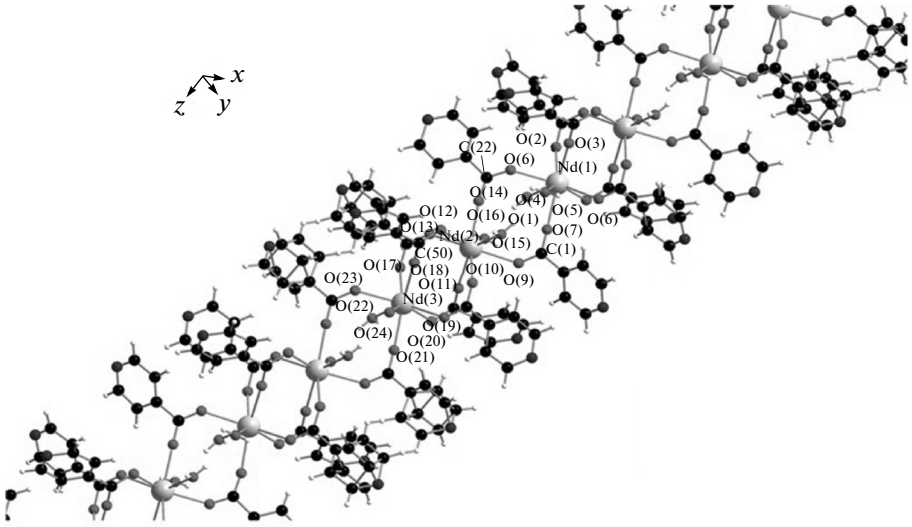

Fig. 2. The coordinated environment of Nd^{3+} ion **I**.

water molecules (Fig. 1a). All nine isonicotinate anions (INA^-) adopt bidentate bridging bonding mode through carboxylate oxygen atoms. This is shown as coordinating mode (a) in Scheme, which illustrates coordination modes of INA^- and NA^- with Nd:

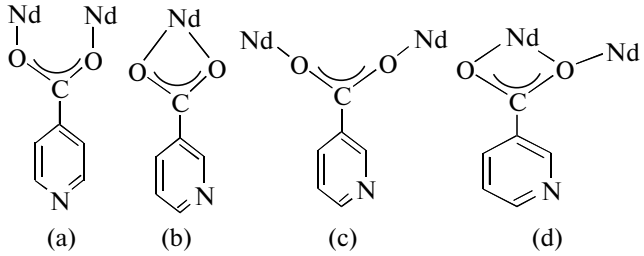

Scheme.

The Nd(1) atom is bonded to eight O atoms, of which six (O(2), O(3), O(5), O(6), O(7), and O(8)) are from six different INA^- species, and two other (O(1) and O(4)) from two water molecules, leading to the formation of a distorted dodecahedral coordination sphere. Nd(1) shares four isonicotinate carboxylates with another neighbouring The Nd(1) atom on one side and two INA^- carboxylates with Nd(2) atom on the other side. The Nd(2) atom besides sharing two INA^- carboxylates with Nd(1) atom on one side, also shares four different units of INA^- carboxylates with Nd(3) atom on the other side (Fig. 2). The Nd(2) atom is also coordinated to two molecules of water to generate a distorted dodecahedral coordination sphere. The distorted dodecahedron is created by six carboxylate oxygens (O(9), O(10), O(11), O(12), O(13), and O(14)) and two oxygen atoms (O(15), O(16)) of two water molecules. The Nd(3) atom in turn completes its eight coordination by sharing two INA^- carboxylates with neighboring Nd(3) atom and also coordinating two water molecules. The coordination environment around Nd(3) atom is also a distorted dodecahedron generated by six INA^- carboxylates oxygen atoms (O(17), O(18), O(19), O(20), O(21), and O(23)) and two oxygen atoms (O(22), O(24)) of two water molecules (Fig. 3a). The Nd–O bond lengths (Table 2) are in the expected range of 2.400(4)–2.467(4) Å [35, 36]. The C-O bonds in all nine bridging carboxylate groups (COO^-) are in the range 1.243(7)–1.258(7) Å indicating resonance between carboxy and carboxylate bonds of isonicotinate anion. The sharing of carboxylate ligand between neighboring Nd^{3+} ions creates a one dimensional coordination polymer with repeated sequence of –Nd(1)–Nd(2)–Nd(3)–Nd(3)–Nd(2)–Nd(1)–Nd(1)–Nd(2)–Nd(3)– (Fig. 4). Adjacent polymer chains are held together by strong hydrogen-bonding and π–π interaction of aromatic pyridine ring (Table 4). This is evident in packing arrangement of polymer as shown in Fig. 5a.

The asymmetric unit of **II** consists of one crystallographically independent Nd^{3+} site, three nicotinate (NA^-) fragments and two coordinated water molecules (Fig. 1b). In the dimer complex, each Nd^{3+} ion is coordinated to seven oxygen atoms of five carboxylate (COO^-) groups of five different NA^- anions. The Nd^{3+} cation is additionally coordinated to two oxygen atom of two water molecules generating a nine coordinated geometry constituted by O(1), O(2), O(3), O(4), O(5), O(6), O*w*(7), O*w*(8). The five NA^- anions coordinate to metal through three different bonding modes (modes b, c and d in Scheme). One NA^- anion is bonded in bidentate chelating mode (mode b) (from O(1) and O(2)) whereas two NA^- anions coordinate as bidentate bridging mode in *syn-syn* configuration

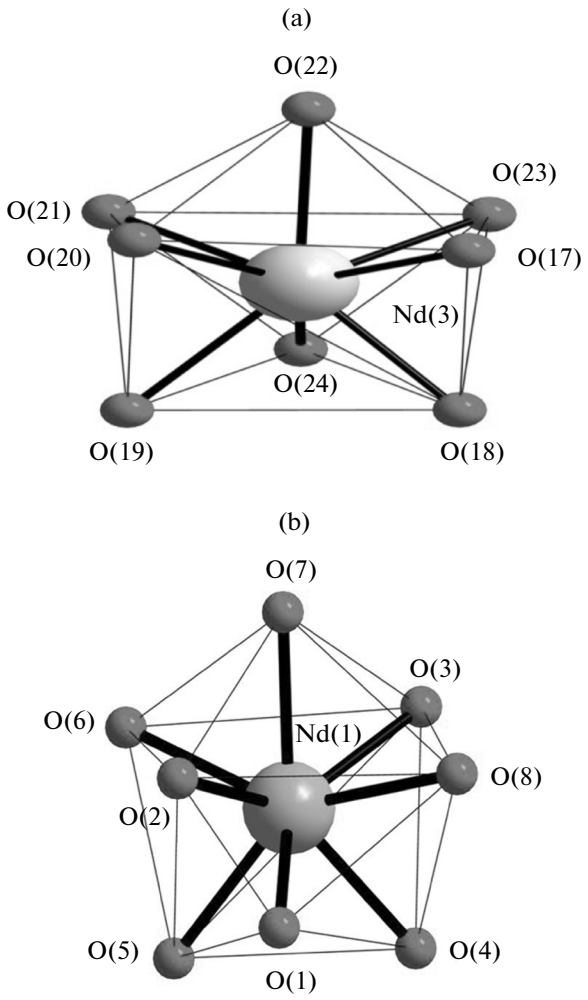

Fig. 3. Distorted dodecahedral view around Nd^{3+} ion in **I** (a) and **II** (b).

(mode c) (through O(4) and O(6)). Two NA^- anions adopt terdentate bridging μ_2-O;κ^2OO' coordination mode (bidentate through O(3) and O(5) toward one Nd^{3+} ion and monodentate across O(5) towards another Nd^{3+} ion, and the atoms symmetry-related) (mode d). The Nd–O bond lengths (Table 3) are in the expected range of 2.409(13)–2.598(13) Å but Nd–O(5) 2.8935(14) μ_2-O bond is exceptionally long and does not seem to affect the coordination geometry around Nd. The OCO bond angles in three differently bonded carboxylate units (bidentate chelating (b), μ_2-O;κ^2OO' mode (d) and bridging mode (c)) are 121.40(17), 122.53(17) and 126.13(17)°, respectively (Table 3). The Nd–O bond lengths are in the expected range as observed in analogous nicotinates of other lanthanides [37]. The polyhedron around Nd has only eight corners and geometry is a distorted dodecahedron (Fig. 3b). Two distorted dodecahedrons are connected to each other through two μ_2-O;κ^2OO' coordination modes of two NA^- ligands and two bidentate bridges of two other NA^- ligands making it a dimeric unit. These dimeric units are packed together through extensive hydrogen-bonding involving N atom of pyridine ring and π–π interaction (Table 4). Packing arrangement of **II** when viewed along *z* axis is shown in Fig. 5b.

The N_2 adsorption isotherm of **I** has a gradual initial uptake due to weak adsorbate–adsorbent interaction and shows hysteresis indicating presence of mesopores (Fig. 6a). The polymer exhibits a type IV isotherm with *type* H4 hysteresis loop [38, 39]. The shapes of hysteresis loops have often been identified with specific pore structures in coordination polymer network [40]. The limiting adsorption at high $P/P°$ indicates capillary condensation taking place within mesopores. Y-intercept 80.36, correlation coefficient 0.999016 and BET C constant 3.182. The value of BET C constant suggests a low heat of adsorption. The Langmuir surface area is found somewhat higher

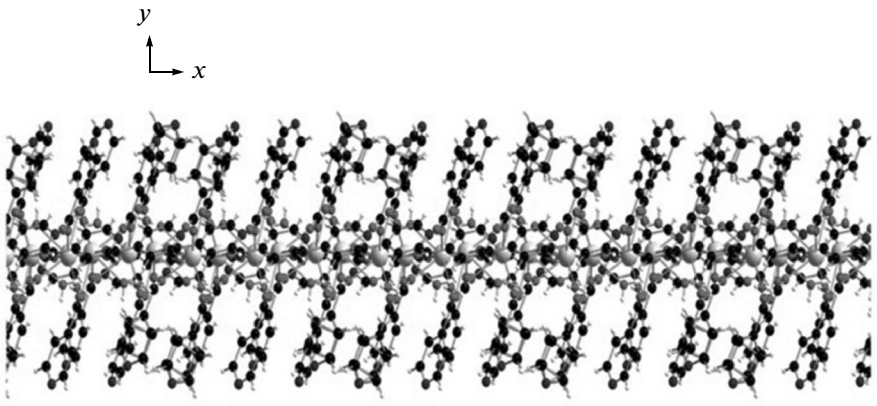

Fig. 4. Polymer expansion of **I** when viewed along *z* axis.

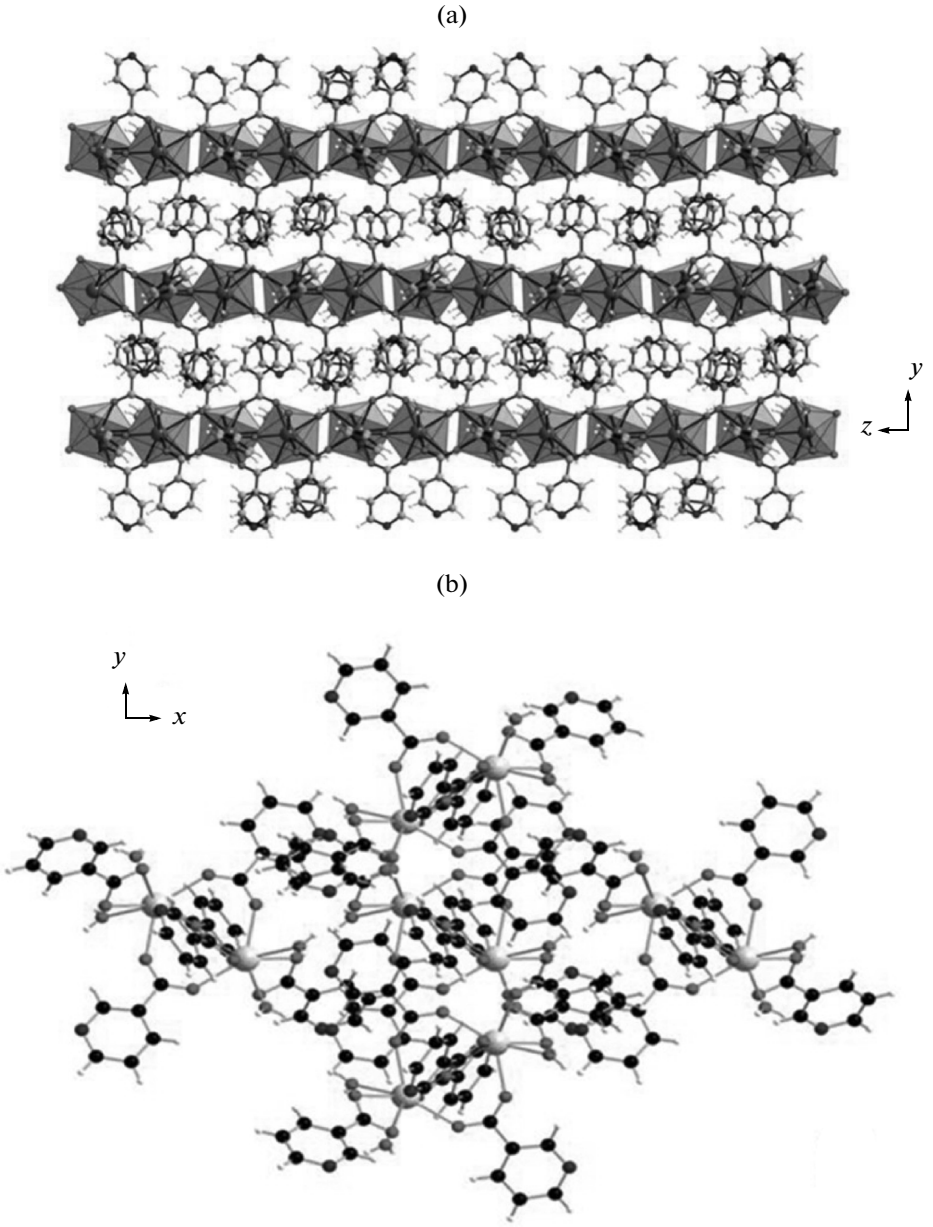

Fig. 5. Packing arrangement of **I** when viewed along *x* axis (a) and **II** when viewed along *z* axis (b).

(94.67 m^2/g) with a slope of 36.79, Y-intercept 84.97, correlation coefficient 0.999400 and Langmuir constant 0.43293. Micropore volume and micropore surface area obtained from *t*-Method Micropore Analysis (de Boer) are 0.010 cm^3/g and 11.53 m^2/g with a Y-intercept 6.53 cc/g and slope 0.1352 (Fig. 6b).

The external surface area is 2.09 m^2/g with a correlation coefficient of 1.000. This is almost the same as the BET surface area. The pore size distribution pattern obtained from desorption branch by employing the BJH model shows wide distribution of pores in the polymer. The pore diameters range from 3 nm to more than 15 nm with an average of 3.96 nmn (Fig. 6c). The total pore volume is 0.1351 cm^3/g for pores smaller than 15 nm at $P/P^\circ = 0.9578$.

To investigate stability of **I** and **II**, TGA–DTA were performed on single crystals samples under N_2 atmosphere with a heating rate of 10°C/min from 0 to 1000°C (Fig. 7). Coordination polymer **I** is thermally robust up to 100°C and starts decomposing from 150°C onwards. The first step of weight loss of ~7% in the temperature range 150–300°C corresponds to the loss of all six water molecules (calcd. 6.59%). This is evident from appearance of two sharp endothermic

Table 4. Geometric parameters of hydrogen bonds for **I** and **II***

D–H···A	Distance, Å			D–H···A, deg
	D–H	D···A	H···A	
		I		
O(1)–H(112)···O(16)^{i}	0.79	2.956	2.163	172
C(7)–H(7)···O(6)^{i}	0.95	3.498	2.713	140
C(28)–H(28)···O(13)^{i}	0.95	3.644	2.811	146
O(15)–H(214)···O(4)^{i}	0.83	3.015	2.202	165
C(42)–H(42)···O(9)^{i}	0.95	3.342	2.448	156
C(52)–H(52)···O(23)^{i}	0.95	3.410	2.543	151
C(60*A*)–H(60*A*)···N(8)^{i}	0.95	3.537	2.683	149
C(31*A*)–H(31*A*)···O(23)^{i}	0.95	3.684	2.822	151
C(32*A*)–H(32*A*)···N(9)^{i}	0.95	3.763	2.856	159
C(11)–H(11)···O(15)^{ii}	0.95	3.517	2.946	119
O(16)–H(215)···N(7)^{ii}	0.79	2.773	1.974	177
C(11)–H(11)···O(12)^{ii}	0.95	3.596	2.827	138
C(11)–H(11)···O(14)^{ii}	0.95	3.799	2.915	155
C(14)–H(14)···O(8)^{iii}	0.95	3.392	2.514	153
C(25)–H(25)···N(2)^{iii}	0.95	3.691	2.962	134
C(18)–H(18)···O(17)^{iv}	0.95	3.408	2.527	154
C(39)–H(39)···O(20)^{v}	0.95	3.493	2.742	136
C(39)–H(39)···O(21)^{v}	0.95	3.661	2.799	151
O(4)–H(114)···N(9)^{vi}	0.86	2.837	1.990	165
O(15)–H(213)···N(8)^{vi}	0.85	2.816	2.008	157
C(48)–H(48)···N(7)^{vi}	0.95	3.540	2.897	126
O(4)–H(113)···N(1)^{vii}	0.80	2.809	2.016	170
C(55)–H(55)···O(1)^{vii}	0.95	3.491	2.927	119
C(55)–H(55)···O(5)^{vii}	0.95	3.543	2.761	140
C(55)–H(55)···O(7)^{vii}	0.95	3.837	2.982	150
C(34)–H(34)···O(10)^{viii}	0.95	3.450	2.680	138
C(63)–H(63)···N(3)^{ix}	0.95	3.756	2.858	157
O(22)–H(312)···O(24)^{x}	0.76	2.986	2.240	167
O(1)–H(111)···N(5)^{xi}	0.79	2.843	2.065	164
O(22)–H(311)···N(2)^{xi}	0.72	2.888	2.207	157
O(16)–H(216)···N(4)^{xi}	0.79	2.794	2.012	166
		II		
O(7)–H(444)···O(2)^{ii}	0.78	2.791	2.016	170
C(3)–H(3)···O(6)^{ii}	0.95	3.606	2.769	147
C(3)–H(3)···O(7)^{ii}	0.95	3.360	2.522	147
C(6)–H(6)···O(3)^{iii}	0.95	3.459	2.752	131
C(10)–H(10)···O(4)^{iv}	0.95	3.499	2.555	172
O(7)–H(333)···N(1)^{iv}	0.79	2.706	1.925	169
C(12)–H(12)···O(1)^{vi}	0.95	3.315	2.404	160
C(16)–H(16)···O(1)^{vii}	0.95	3.629	2.749	154
C(18)–H(18)···O(2)^{viii}	0.95	3.602	2.760	148
C(18)–H(18)···O(7)^{viii}	0.95	3.484	2.746	135
O(8)–H(222)···N(3)^{ix}	0.78	2.736	1.953	173
O(8)–H(111)···N(2)^{x}	0.79	2.851	2.117	154

* Symmetry codes: ^{i} x, y, z; ^{ii} $x+1, y, z$; ^{iii} $-x+1, -y+2, -z$; ^{iv} $-x+1, y+1/2, -z+1/2$; ^{v} $-x+1, -y+2, -z+1$; ^{vi} $-x, y+1/2, -z+1/2$; ^{vii} $x-1, y, z$; ^{viii} $-x, y-1/2, -z+1/2$; ^{ix} $x, -y+3/2, z+1/2$; ^{x} $-x, -y+2, -z+1$; ^{xi} $-x+1, y-1/2, -z+1/2$ for **I** and ^{i} x, y, z; ^{ii} $-x+1, -y, -z$; ^{iii} $x, -y+1/2, z+1/2$; ^{iv} $x, -y+1/2, z-1/2$; ^{v} $-x+2, y-1/2, -z-1/2$; ^{vi} $-x+2, -y, -z$; ^{vii} $-x+2, -y+1, -z$; ^{viii} $x+1, y, z$; ^{ix} $x-1, y, z$; ^{x} $-x+2, y+1/2, -z-1/2$ for **II**.

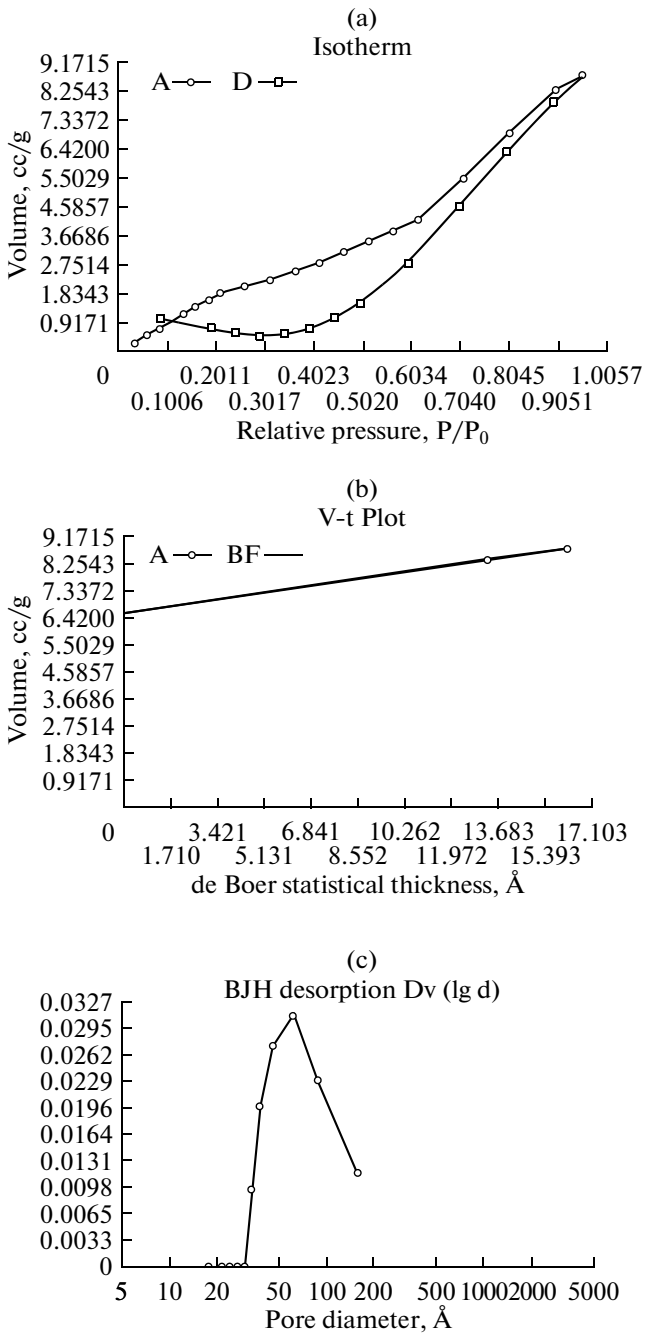

Fig. 6. N_2 adsorption isotherm (a), t-plot analysis (b) and BJH pore size distribution model for **I** (c).

peaks in DTA curve at 200 and 300°C. The anhydrous product remains stable upto 350°C and then the framework breaks down abruptly. This is reflected by steep slope of TGA curve in the temperature range 350–500°C. The decomposition of ligands is evident from sharp exothermic peak in DTA curve at 400°C. The decomposition of ligands continues up to 1000°C when stable oxide of metal Nd_2O_3 is formed. Coordination complex **II** decomposes rather abruptly from 98°C onwards. The whole complex decomposes in single step up to 438°C. The DTA curve shows sharp endothermic peaks around 200, 300, and 400°C. A sharp exothermic peak around 430°C indicates decomposition of ligand.

ACKNOWLEDGMENTS

We thank Sophisticated Analytical Instrumentation Facility, CIL and UCIM Panjab University for FTIR study. Authors are grateful to Dr. Shaikh M. Mobin,

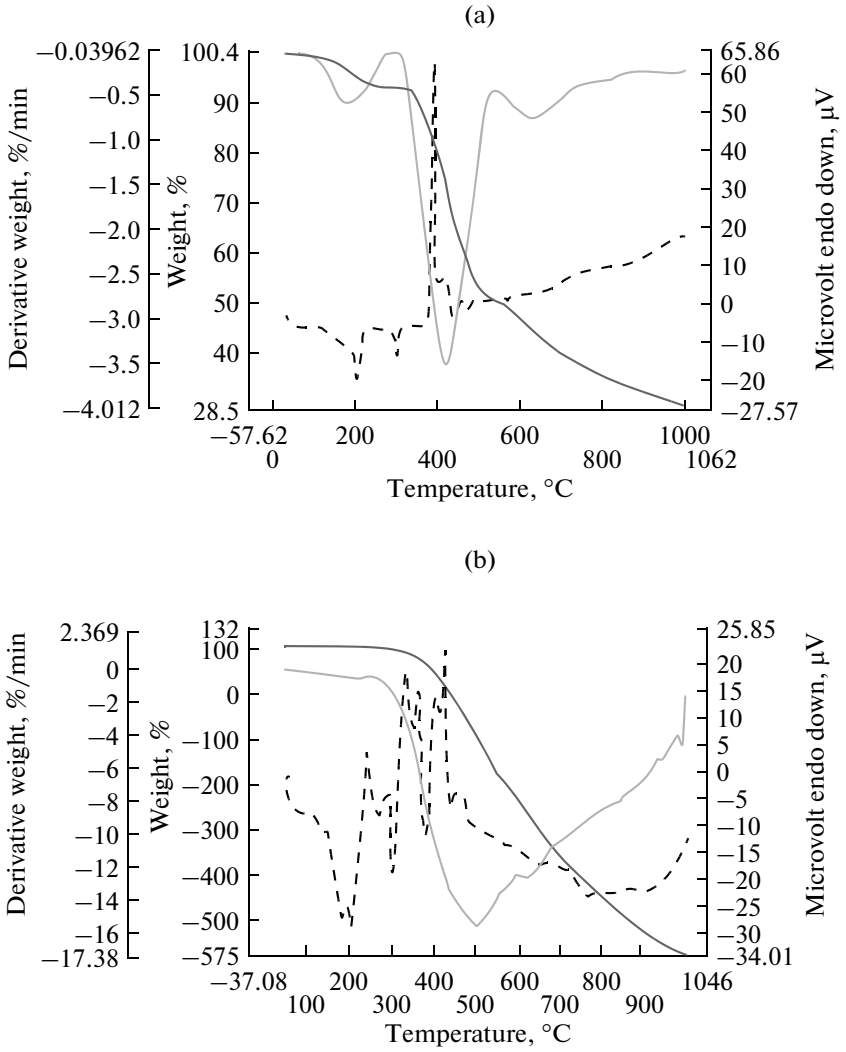

Fig. 7. TGA–DTA curve of **I** (a) and **II** (b).

Incharge, Sophisticated Instrumentation Centre (SIC), Indian Institute of Technology Indore (IITI), M.P. India for single crystal X-ray diffraction study.

REFERENCES

1. Edelmann, F.T., *Chem. Soc. Rev.*, 2012, vol. 41, no. 23, p. 7649.
2. D'Vries, R.F., Iglesias, M., Snejko, N., et al., *J. Mater. Chem.*, 2012, vol. 22, no. 3, p. 1191.
3. Bennett, S.D., Core, B.A., Blake, M.P., et al., *Dalton Trans.*, 2014, vol. 43, no. 15, p. 5871.
4. Roy, S., Chakraborty, A., and Maji, T.K., *Coord. Chem. Rev.*, 2014, vols. 273–274, p. 139.
5. Li, J.-R., Sculley, J., and Zhou, H.-C., *Chem. Rev.*, 2012, vol. 112, no. 2, p. 869.
6. Kurzen, H., Bovigny, L., and Bulloni, C., *Chem. Phys. Lett.*, 2013, vol. 574, p. 129.
7. Huang, W., Wu, D., Zhou, P., et al., *Cryst. Growth Des.*, 2009, vol. 9, no. 3, p. 1361.
8. Song, X.-Q., Zang, Z.-P., Liu, W.-S., et al., *J. Solid State Chem.*, 2009, vol. 182, no. 4, p. 841.
9. Zhang, J., Zheng, B., Zhao, T., et al., *Cryst. Growth Des.*, 2014, vol. 14, no. 5, p. 2394.
10. Guo, X., Zhu, G., Sun, F., et al., *Inorg. Chem.*, 2006, vol. 45, no. 6, p. 2581.
11. Cui, Y., Yue, Y., Qian, G., et al., *Chem. Rev.*, 2012, vol. 112, no. 2, p. 1126.
12. Decadt, R., Hecke, K.V., Depla, D., et al., *Inorg. Chem.*, 2012, vol. 51, no. 21, p. 11623.
13. He, H., Ma, H., Sun, D., et al., *Cryst. Growth Des.*, 2013, vol. 13, no. 3, p. 3154.
14. Yang, J., Lu, N., Zhang, G., et al., *Polyhedron*, 2008, vol. 27, nos. 9–10, p. 2119.
15. Liu, Y.-Fu., Hou, G.-F., Yu, Y.-H., et al., *Cryst. Growth Des.*, 2013, vol. 13, no. 8, p. 3816.
16. Truman, L.K., Comby, S., and Gunnlaugsson, T., *Angew. Chem. Int. Ed.*, 2012, vol. 51, p. 9624.
17. Wang, R., Selby, H.D., Liu, H., et al., *Inorg. Chem.*, 2002, vol. 41, no. 2, p. 278.

18. Fomina, I.G., Dobrokhotova, Z.V., Ilyukhin, A.B., et al., *Polyhedron*, 2013, vol. 65, p. 152.
19. Jiang, H.-L., Makal, T.A., and Zhou, H.-C., *Coord. Chem. Rev.*, 2013, vol. 257, nos. 15–16, p. 2232.
20. Du, Z.Y., Xu, H.B., and Mao, J.G., *Inorg. Chem.*, 2006, vol. 45, no. 24, p. 9780.
21. Feng, R., Jiang, F.L., Wu, M.Y., et al., *Cryst. Growth Des.*, 2010, vol. 10, no. 5, p. 2306.
22. Xu, N., Wang, C., Shi, W., et al., *Eur. J. Inorg. Chem.*, 2011, vol. 2011, no. 15, p. 2387.
23. Sun, X.-L., Shen, B.-X., Zang, S.-Q., et al., *CrystEngComm*, 2013, vol. 15, no. 26, p. 5910.
24. Zeng, Y.-F., Hu, X., Liu, F.-C., et al., *Chem. Soc. Rev.,* 2009, vol. 38, p. 469.
25. Cheng, L., Zhang, W.-X., Ye, B.-H., et al., *Eur. J. Inorg. Chem.*, 2007, vol. 2007, no. 18, p. 2668.
26. Liu, F.-C., Zeng, Y.-F., Zhao, J.-P., et al., *Inorg. Chem.*, 2007, vol. 46, no. 19, p. 7698.
27. Wang, X.-Y. and Sevov, C., *Chem. Mater.*, 2007, vol. 19, no. 15, p. 3763.
28. Mahata, P., Ramya, K.V., and Natarajan, S., *Chem. Eur. J.*, 2008, vol. 14, no. 19, p. 5839.
29. Wang, X.-Y., Wang, Z.-M., and Gao, S., *Chem. Commun.*, 2008, vol. 12, no. 4, p. 281.
30. Sanotra, S., Gupta, R., Khajuria, S., et al., *J. Inorg. Organomet. Polym.*, 2013, vol. 23, no. 4, p. 897.
31. Sheldrick, G.M., *SHELXS-97, Program for Crystal Structure Solution*, Göttingen (Germany): Univ. of Göttingen, 1997.
32. Sheldrick, G.M., *SHELXL-97, Program for Crystal Structure Refinement*, Göttingen (Germany): Univ. of Göttingen, 1997.
33. Deacon, G.B. and Phillips, R.J., *Coord. Chem. Rev.*, 1980, vol. 33, no. 3, p. 227.
34. Feng, L.S., Chen, Z., Zeller, M., et al., *Inorg. Chim. Acta*, 2013, vol. 394, p. 729.
35. Xu, J., Su, W., and Hang, M., *Inorg. Chem. Commun.*, 2011, vol. 14, no. 11, p. 1794.
36. Chen, S., Fan, R.-Q., Sun, C.-F., et al., *Cryst. Growth Des.*, 2012, vol. 12, no. 3, p. 1337.
37. Mao, J.-G., Zhang, H.-J., Ni, J.-Z., et al., *Polyhedron*, 1998, vol. 17, nos. 23–24, p. 3999.
38. Gelb, L.D., Gubbins, K.E., Radhakrishnan, R., et al., *Rep. Prog. Phys.*, 1999, vol. 62, no. 12, p. 1573.
39. Lowell, S., Shields, J.E., Thomas, M.A., et al., *Characterisation of Porous Solid and Powders: Surface Area, Pore Size and Density*, Kluwer Academic Publ., 2004.
40. Singh, K., Everett, D., Haul, R., et al., *Pure Appl. Chem.*, 1985, vol. 57, no. 4, p. 603.